

RESEARCH

Open Access



Translocation of the *Alphanucleorhabdovirus* X proteins from the cytoplasm into the nucleus through interaction with nucleocapsid protein is essential for viral pathogenesis

Shuo Wang^{1,2,3}, Shuang Ni^{1,2,3}, Huanhuan Lou^{1,2,3}, Yan Liang^{1,2,3} and Zhenghe Li^{1,2,3*} 

Abstract

The diverse rhabdoviruses infecting plants and animals have conserved genome organizations, and the functions of viral structural proteins have been extensively studied. However, increasing number of rhabdoviruses have been found to encode various accessory proteins, whose specific roles during viral infection remain poorly understood. In this study, we investigated the function of the X proteins encoded by several members of the genus *Alphanucleorhabdovirus*. Using the recently established eggplant mottled dwarf virus (EMDV) reverse genetics system, we found that recombinant EMDV lacking the X gene was able to systemically infect *Nicotiana benthamiana* plants, albeit with reduced efficiency. However, this deletion mutant was largely restricted to the veinal tissues and caused asymptomatic infections. The EMDV X protein, which localized to the cytoplasm when expressed alone, was translocated to the nucleus via a specific interaction with the nucleocapsid (N) protein. Through analyzing the interactions of the X deletion mutants and the infection phenotypes of the derived EMDV deletion mutants, we demonstrated that the carboxyl-terminal region of the X protein (amino acids 71–83) is crucial for its interaction with the N protein and for viral pathogenesis. Moreover, the X proteins encoded by related alphanucleorhabdoviruses could fully or partially complement the functions of EMDV X in viral infection. These findings provide new insights into the roles of accessory proteins in plant rhabdovirus infection.

Keywords Eggplant mottled dwarf virus, Plant rhabdovirus, Nucleorhabdovirus, X protein, Accessory protein, Reverse genetics system

Background

The family *Rhabdoviridae* is an ecologically diverse group comprising hundreds of virus members infecting plants or animals, many of which are transmitted by arthropod vectors (Kuzmin et al. 2009; Dietzgen et al. 2020). The genomes of rhabdoviruses consist of single-stranded, negative sense RNAs encoding five conserved structural proteins: nucleocapsid protein (N), phosphoprotein (P), matrix protein (M), glycoprotein (G), and large polymerase protein (L), in the order of 3'-N-P-M-G-L-5'. In addition to these canonical structural proteins, various rhabdovirus lineages encode additional accessory

*Correspondence:
Zhenghe Li
lizh@zju.edu.cn

¹ State Key Laboratory of Rice Biology, Institute of Biotechnology, Zhejiang University, Hangzhou 310058, China

² Ministry of Agriculture Key Laboratory of Molecular Biology of Crop Pathogens and Insect Pests, Zhejiang University, Hangzhou 310058, China

³ Key Laboratory of Biology of Crop Pathogens and Insects of Zhejiang Province, Zhejiang University, Hangzhou 310058, China



proteins, which can exist as independent transcription units or as alternative, overlapping, or consecutive open reading frames (ORFs) within major structural protein genes (Walker et al. 2011, 2015; Bejerman et al. 2023). These accessory proteins, typically present in a clade-specific manner, generally displayed negligible amino acid sequence similarity to other known proteins (Walker et al. 2015).

Although putative accessory genes can be found in each of the structural protein gene junctions, the P-M gene junction often contains orthologous sets of accessory genes in specific rhabdovirus clades (Walker et al. 2015). For instance, plant rhabdoviruses contain a P3 ORF between the *P* and *M* genes, which codes for a movement protein required for intracellular and intercellular trafficking of viral nucleocapsids (Huang et al. 2005; Wang et al. 2015; Mann et al. 2016; Zhou et al. 2019). Within the *P-M* gene junction, three additional ORFs (P4, P5, and P6) exist in several closely related plant cytorhabdoviruses, including barley yellow striate mosaic virus (BYSMV), northern cereal mosaic virus, and maize yellow striate virus (Yan et al. 2015; Maurino et al. 2018). BYSMV P5 protein is a small transmembrane protein with unknown function (Yan et al. 2015), whereas P6 functions to increase host attractiveness to insect vectors through inhibiting the jasmonic acid signaling pathway (Gao et al. 2022) and to induce hyperactivity of the insect vector to prolong the duration of phloem feeding and virus transmission (Gao et al. 2023). Similarly, members in the genus *Hepavirus*, a group of vertebrate-infecting viruses transmitted by arthropod vectors, also contain one to four accessory ORFs encoding small proteins with unknown function, although none of these proteins shares sequence similarities with the plant rhabdovirus P3 proteins (Walker et al. 2015).

The *G-L* gene junction appears to be another hot spot for housing accessory genes. Members in the genera *Almendravirus*, *Bahiovirus*, *Curiovirus*, *Ephemerovirus*, *Hapavirus*, and *Tibrovirus* contain one or more accessory ORFs between the *G* and *L* genes, one of which encodes a small hydrophobic protein resembling class IA viroporins (Walker et al. 2015). These small proteins exhibit a highly conserved structure featuring a predicted N-terminal ectodomain with clusters of aromatic residues, a central transmembrane domain and a highly basic C-terminal domain (McWilliam et al. 1997). Expression of the $\alpha 1$ protein of bovine ephemeral fever ephemerovirus increased cell membrane permeability, confirming its viroporin activity (Joubert et al. 2014). An accessory ORF located in this position, referred to P6 or P9 in many plant-infecting cytorhabdoviruses, has also been described to encode a small, predicted transmembrane protein sharing structural characteristics of viroporin

(Bejerman et al. 2021, 2023). Indeed, BYSMV P9, as well as its orthologs in several related cytorhabdoviruses, has recently been demonstrated to have potassium-conducting viroporin activities, facilitating virion disassembly (Gao et al. 2024). Despite the aforementioned findings, the functions of most accessory proteins remain uncharacterized.

The genus *Alphanucleorhabdovirus* is comprised of a monophyletic cluster of plant-infecting members that replicate and undergo virion morphogenesis in the nuclei of infected cells (Walker et al. 2022). Several closely related alphanucleorhabdoviruses, including eggplant mottled dwarf virus (EMDV), *Physostegia* chlorotic mottle virus (PhCMoV), potato yellow dwarf virus (PYDV), constricta yellow dwarf virus (CYDV), and joá yellow blotch-associated virus, have a distinguishing genome organization characterized by a small 'X' ORF located between the *N* and *P* genes (Mavrič et al. 2006; Alfaro-Fernández et al. 2011; Bandyopadhyay et al. 2010; Babaie et al. 2014; Jang et al. 2017; Menzel et al. 2018; Dietzgen et al. 2021a, b). The X proteins lack significant sequence identities with any known proteins or conserved motifs that could suggest its potential functions in virus infection cycle.

In this study, we set out to investigate the X protein functions using the recently developed EMDV reverse genetics system (Wang et al. 2024). We found that the EMDV X protein is a non-virion protein required for efficient plant infection and symptom induction. During EMDV infection, X protein is relocated from the cytoplasm into the nucleus through an interaction with the N protein, enhancing the pathogenicity of EMDV. Furthermore, the functions of EMDV X can be complemented by paralogs encoded by related alphanucleorhabdoviruses, suggesting functional conservation among X proteins.

Results

EMDV X is a nonstructural protein required for efficient infection and symptom induction

We utilized a green fluorescent protein (GFP)-tagged, wild-type EMDV infectious clone (referred to as EMDV X_{WT}) (Wang et al. 2024) to determine the role of the X protein in EMDV infection through analyzing the phenotypes of the X deletion mutant virus. To this end, we substituted the red fluorescent protein (*RFP*) gene for X gene or fused RFP in frame to the N-terminus of the X gene, generating EMDV RdX and EMDV R-X, respectively (Fig. 1a). All EMDV clones were successfully recovered through agroinfiltration of *Nicotiana benthamiana* plants, as evidenced by recombinant virus infections at 30 days post inoculation (dpi) (Fig. 1b). However, the infectivity of EMDV RdX was significantly lower (36.7%) compared with EMDV X_{WT} (86.7%) or EMDV

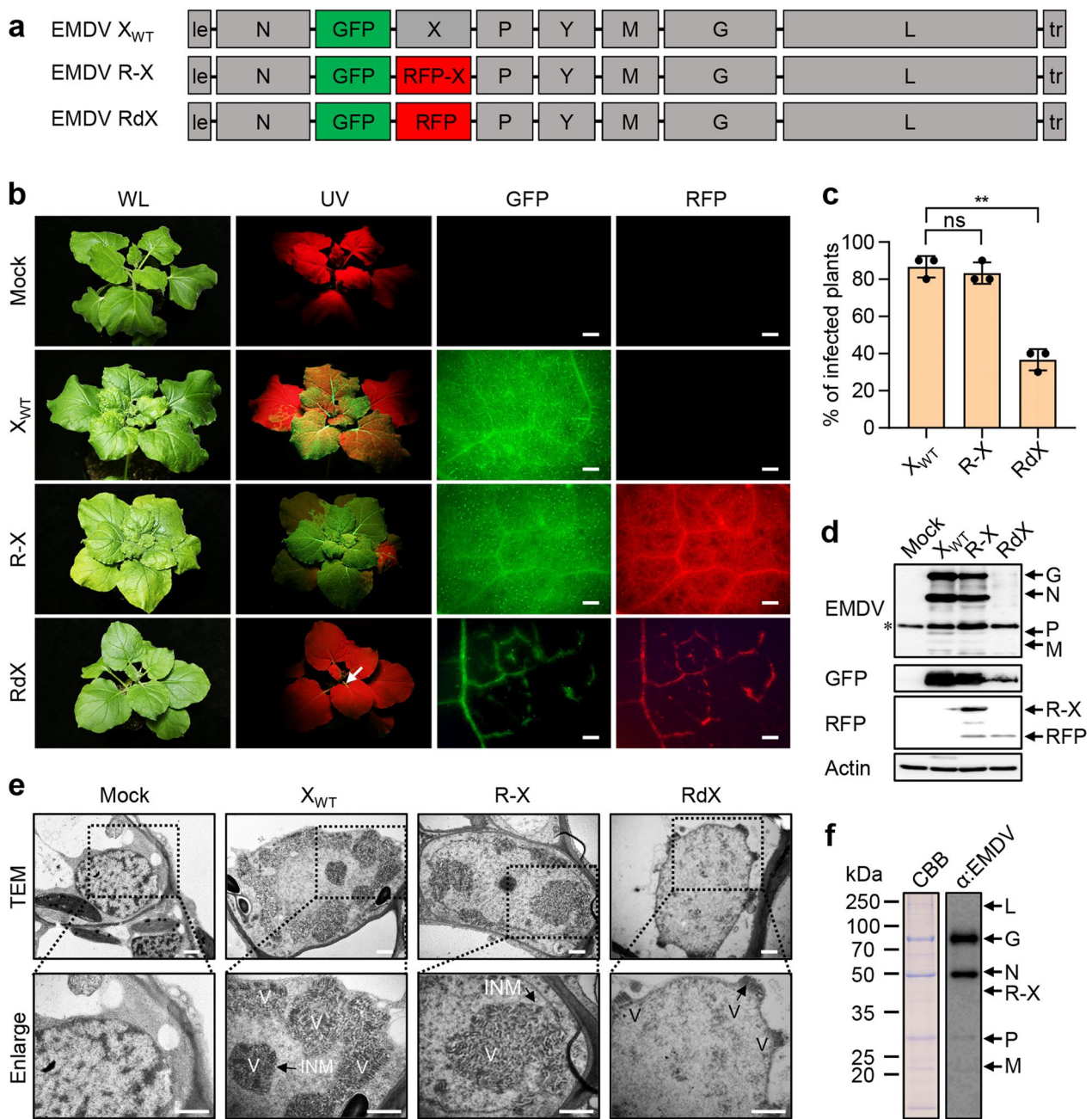


Fig. 1 Effects of the X protein deletion and RFP fusion on EMDV infection of *N. benthamiana* plants. **a** Schematic representation of the recombinant EMDV X_{WT} , EMDV R-X, and EMDV RdX genomes. **b** Symptoms and fluorescence in *N. benthamiana* plants systemically infected with recombinant EMDV derivatives. Infected plants were photographed at 30 days post inoculation (dpi) under white light (WL) or ultraviolet (UV) illumination with a stereo fluorescence microscope. Arrow indicates an infected leaf petiole with faint GFP fluorescence. Scale bars: 500 μ m. **c** Percentages of systemically infected *N. benthamiana* plants with the indicated EMDV clones at 30 dpi. Data are shown as individual data points and mean \pm SD for 3 independent experiments ($n = 10$). Statistical comparison was performed via two-tailed Student's t -test (**, $P < 0.01$; ns, $P > 0.05$ not significant). **d** Western blot analysis of the expression of viral structural and fluorescent proteins in leaf tissues infected with recombinant EMDV. The actin blot serves as a protein loading control. Asterisk indicates a non-specific band. **e** Transmission electron micrographs showing the nuclei infected with indicated EMDV virus. The boxed sectors are magnified at the lower panels. V, virion; INM, inner nuclear membrane. Scale bars: 1 μ m. **f** Detection of RFP-X in virus particles purified from *N. benthamiana* plants infected with EMDV R-X. The purified virion preparation separated by SDS-PAGE were stained with Coomassie brilliant blue and blotted with a polyclonal antiserum raised against EMDV virions. Protein ladders are indicated at the left side of the CBB panel. Positions of EMDV structural and fluorescent proteins are marked at the right side of the image

R-X (83.3%) (Fig. 1c). Fluorescence microscopy revealed extensive fluorescence in the veins and mesophyll tissues of upper leaves infected with EMDV X_{WT} or EMDV R-X, whereas EMDV RdX-infected leaves exhibited weak fluorescence, primarily restricted to the major and minor veins (Fig. 1b). Unlike the typical leaf crinkling and vein clearing symptoms associated with EMDV X_{WT} or EMDV R-X infections, *N. benthamiana* plants infected with EMDV RdX were nearly symptomless (Fig. 1b). Symptom severity correlated with viral protein accumulation levels; abundant EMDV structural proteins were present in EMDV X_{WT} and EMDV R-X leaf tissues, while only low levels of viral proteins and fluorescence proteins were detected in the EMDV RdX-infected tissues (Fig. 1d). Taken together, these data demonstrate that the X protein plays a crucial role in EMDV infection and symptom development, and the N-terminal RFP fusion does not alter the X protein expression and function.

To further investigate the role of the X protein, we employed transmission electron microscopy to analyze virion morphogenesis and the cytopathology associated with recombinant EMDV infections. As anticipated, numerous bacilliform particles were present in the nuclei infected with EMDV X_{WT} or EMDV R-X, often occurring as irregular clusters and surrounded by invaginated inner nuclear membranes. In contrast, only a few bacilliform virions in EMDV RdX-infected nuclei were found to accumulate in the perinuclear spaces, and inner nuclear membrane invagination was rarely observed (Fig. 1e). We then purified EMDV R-X particles to determine whether the X protein constitutes a structural component of the virion. EMDV R-X was used for this analysis because this virus behaves similarly to EMDV X_{WT} and contains an RFP-tagged X, facilitating its detection. Coomassie brilliant blue staining of purified virion preparations identified proteins consistent with the five known structural proteins (L, G, N, P, and M), but a protein with a predicted size of RFP-X (approximately 36.8 kDa) was not detected. Additionally, polyclonal antiserum raised against EMDV virions failed to detect the presence of RFP-X in the virion preparations (Fig. 1f). Thus, the data obtained suggest that the X protein is not present in purified EMDV virions at a detectable level.

EMDV X is translocated from the cytoplasm to the nucleus through interacting with the N protein

To determine the subcellular localization of the EMDV X protein, we transiently expressed the N-terminal GFP and RFP fusion of X (GFP-X and RFP-X) in the leaves of *N. benthamiana* RFP-H2B and 16c lines, which transgenically express the RFP-fused nuclear marker histone 2B and the endoplasmic reticulum (ER) lumen-targeting mGFP5 protein, respectively (Haseloff and Siemering 2006; Martin et al. 2009). Confocal microscopy revealed that the X fluorescence was present exclusively in the cytoplasm and colocalized with the reticular structure of the ER (Fig. 2a, b). Nuclear-cytoplasmic fractionation confirmed the cytoplasmic localization of the transiently expressed GFP-X (Fig. 2c, left panels). Subcellular fractionation and microsome association analyses showed that RFP-X was present exclusively in the P30 membrane fraction (Additional file 1: Figure S1a), similar to the plasma membrane intrinsic protein 2A fused to RFP (PIP2A-RFP) (Yamada et al. 2005). Upon treatments of the P30 fractions with 0.1 M Na₂CO₃ or 4 M urea, RFP-X was partially released into the soluble fraction (Additional file 1: Figure S1b). These results, combined with the absence of transmembrane domains in X as predicted by bioinformatics software, suggest that EMDV X is a membrane-associated protein rather than an integral membrane protein.

The subcellular localization of rhabdovirus proteins often differs upon ectopic expression and in the context of virus infections (Dietzgen et al. 2021a, b). During EMDV R-X infection, we found that a significant fraction of RFP-X was translocated into the nucleus, as revealed by confocal microscopy (Fig. 2d), and further confirmed by nuclear-cytoplasmic fractionation (Fig. 2c, right panels). These observations suggested that other viral proteins might redirect X to the nucleus. To test this hypothesis, GFP-X was co-expressed with cyan fluorescent protein (CFP)-fused N, P, Y or M proteins in the leaves of RFP-H2B *N. benthamiana* plants. Notably, although all CFP fusions exhibited partial or exclusive nuclear localization, only N was able to relocate GFP-X to the nucleus (Fig. 2e). Since CFP fusion to EMDV L was undetectable due to its large size, we co-expressed the

(See figure on next page.)

Fig. 2 Subcellular localization of the EMDV X protein. **a, b** Subcellular localization of the transiently expressing GFP-X in epidermal cells of *N. benthamiana* plants transgenic for RFP-H2B, and RFP-X in 16c line transgenic for the ER-targeting mGFP5. Confocal micrographs were captured at 48 h post agroinfiltration (hpi). **c** Nucleocytoplasmic distribution assay of the transiently expressed GFP-X (left) and RFP-X expressed during EMDV R-X infection (right). Histone H3 or actin served as the nuclear or cytoplasmic marker, respectively. **d** Confocal micrographs showing the localization of RFP-X and RFP expressed during EMDV R-X and EMDV RdX infections. **e** Confocal micrographs showing the subcellular localization of GFP-X co-expressed with each CFP-tagged EMDV proteins or the untagged L protein in epidermal cells of *N. benthamiana* RFP-H2B transgenic plants. Confocal micrographs were captured at 48 hpi. Zoom-up views of boxed areas were presented to show the fluorescence patterns in the nuclei. Scale bars: 20 μm

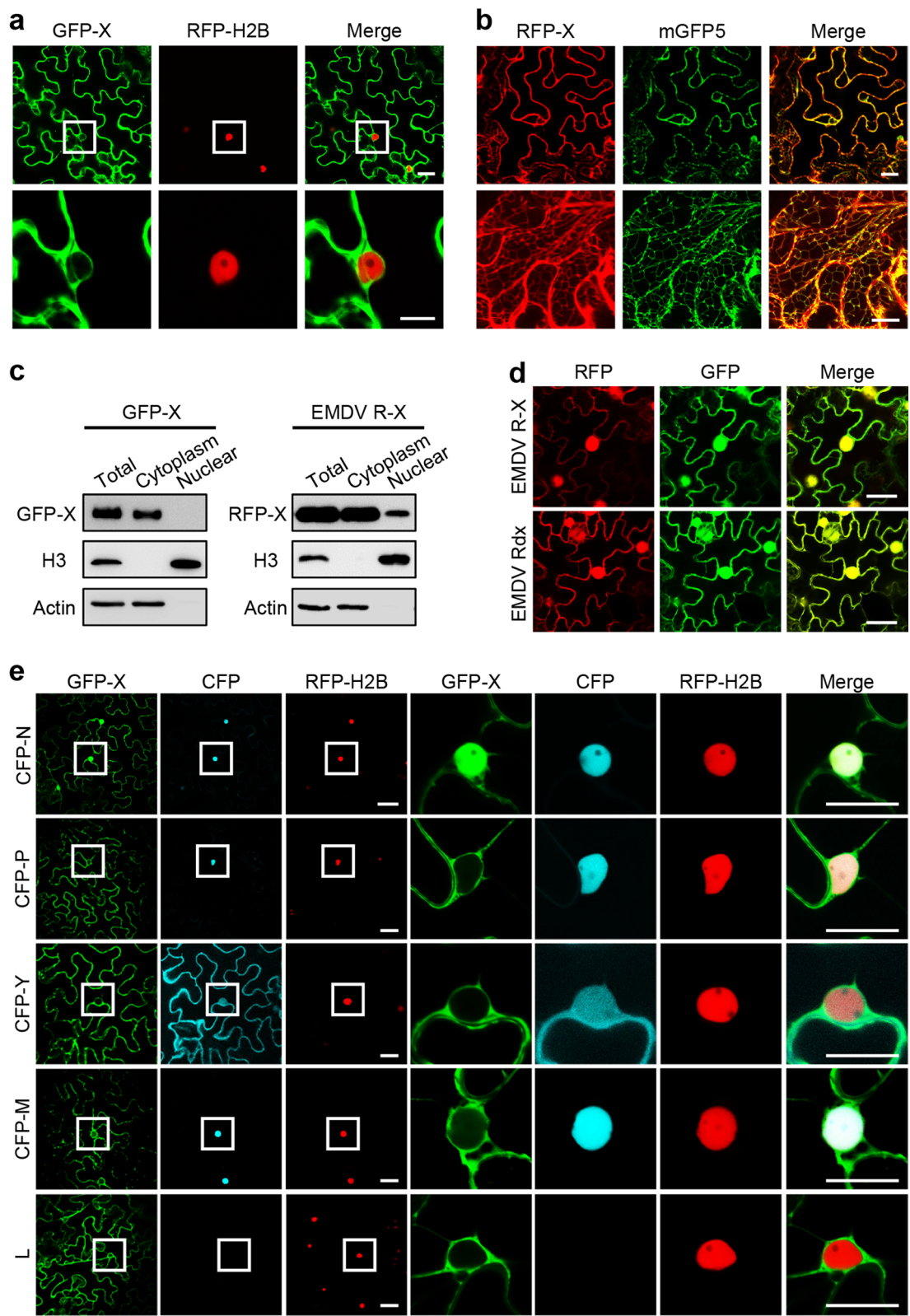


Fig. 2 (See legend on previous page.)

untagged L protein whose expression had been functionally verified in the recombinant EMDV recovery experiments (Wang et al. 2024). However, L failed to redirect the co-expressed GFP-X protein to the nucleus (Fig. 2e). These findings indicate that during EMDV infection the N protein mediates the redistribution of X from the cytoplasm to the nucleus.

EMDV X protein interacts with the N protein through its carboxyl terminus

To investigate the possible interaction between EMDV X and N proteins, we conducted a bimolecular fluorescence complementation (BiFC) assay. This was achieved by co-expressing X fused to the yellow fluorescent protein (YFP) C-terminal domain (Y^C-X) and N fused to the YFP N-terminal domain (Y^N-N) in the leaves of RFP-H2B *N. benthamiana* plants. Confocal microscopy revealed the X-N interaction fluorescence signals in both the

cytoplasm and nucleus (Fig. 3b). Further validation of the X-N interaction was obtained through a co-immunoprecipitation (Co-IP) assay using proteins extracted from *N. benthamiana* leaves co-expressing GFP-tagged N (GFP-N) and RFP-X (Fig. 3c). Additionally, a GST pull-down assay was performed using GST-tagged X (GST-X) and 6×histidine (HIS)-tagged N (HIS-N) expressed in *Escherichia coli* cells, which confirmed a direct interaction between EMDV X and N proteins (Fig. 3d).

EMDV X is a small protein consisting of 96 amino acids (aa). Using AlphaFold2-based structural modeling, we divided the X protein into an N-terminal domain (X_{NT}, aa 1–43) composed of an alpha-helix, and a C terminal domain (X_{CT}, aa 44–96) comprising two short beta-strands and an alpha-helix (Fig. 3a). Subcellular localization analyses showed that the RFP-X_{NT} fusion was targeted to the cytoplasm exclusively, whereas the RFP-X_{CT} fusion was present in both the cytoplasm and the

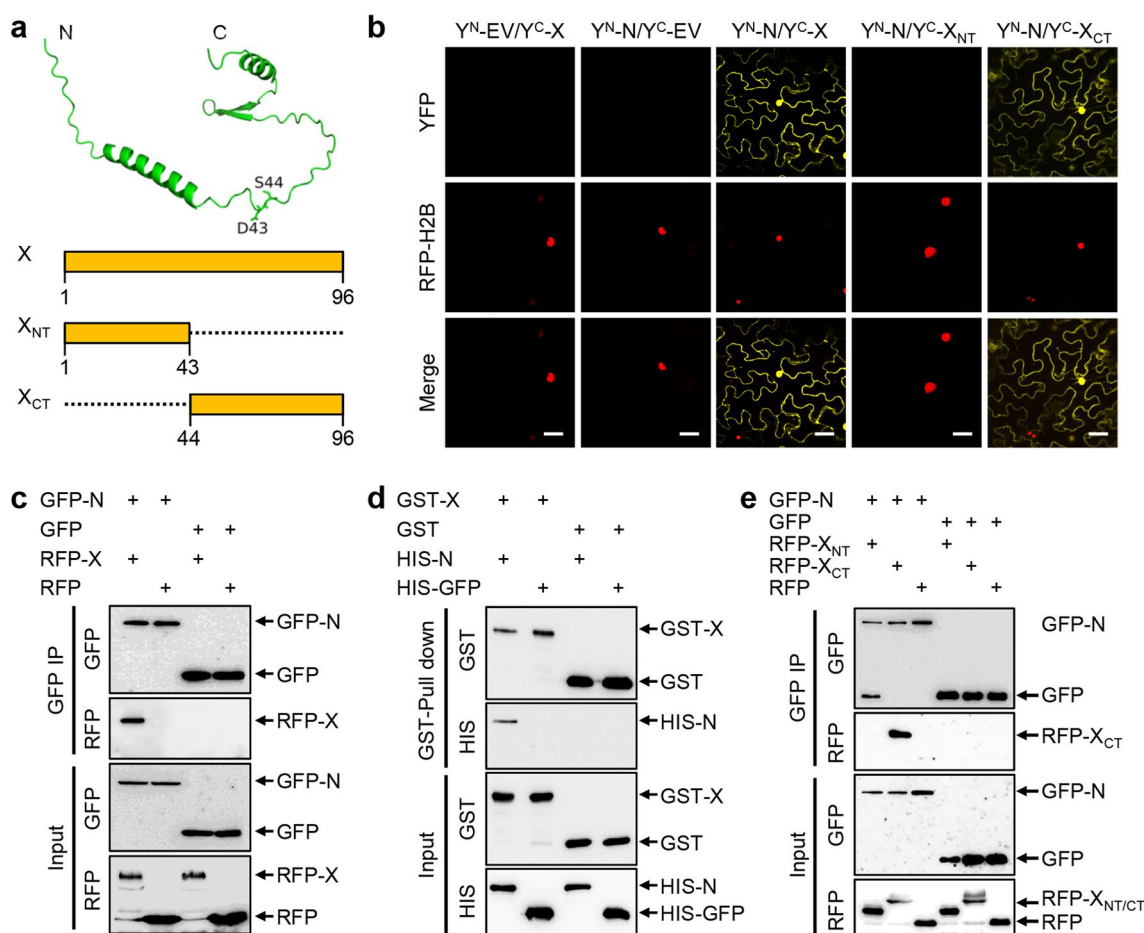


Fig. 3 Interactions between the EMDV X and N proteins. **a** The structure of EMDV X modelled by AlphaFold2 (<https://colab.research.google.com/>) and schematic domain demarcation. Dash lines denote the truncation. **b** BiFC assays to determine the interactions between EMDV N and X derivatives. Leaves of *N. benthamiana* RFP-H2B plants were agroinfiltrated to co-express Y^N-N with Y^C-X, Y^C-X_{NT}, and Y^C-X_{CT}, respectively. Confocal micrographs were captured at 48 hpi. **c, e** Co-IP assays for analyzing the interactions between EMDV N and the full-length X protein or its truncation mutants. **d** GST-Pull down assay for analyzing the interactions between N with X

nucleus (Additional file 1: Figure S2). BiFC and Co-IP assays were employed to determine the specific domain of the X protein responsible for the interaction with N. The results showed that the X_{CT}, but not the X_{NT}, specifically interacts with the N protein (Fig. 3b, e). In summary, these data demonstrated that the EMDV X protein directly interacts with the N protein through its C terminus.

Requirements of the X protein domains in EMDV pathogenicity

To elucidate the roles of the X protein domains in EMDV infection, we introduced truncations of the X_{NT} and X_{CT} domains into the EMDV R-X clone, generating EMDV R-X_{NT} and EMDV R-X_{CT}, respectively. *N. benthamiana* plants agroinoculated with EMDV R-X_{NT} were symptomless and exhibited localized GFP and RFP distribution

similar to those observed in EMDV RdX infections (Fig. 4a). In contrast, plants infected with EMDV R-X_{CT} exhibited stunting, leaf crinkling, and vein clearing symptoms, along with widespread fluorescence (Fig. 4a), resembling infections caused by EMDV-X_{WT} (Fig. 1a).

Western blot analysis revealed that EMDV R-X_{NT} accumulated at low levels in infected plants, while EMDV R-X_{CT} infections produced abundant structural proteins comparable to those in EMDV R-X infections (Fig. 4b). Surprisingly, both EMDV R-X_{NT} and EMDV R-X_{CT} displayed poor infectivity similar to EMDV-RdX, but significantly lower than EMDV R-X (Fig. 4c). During recombinant EMDV infections, RFP-X_{NT} was localized exclusively to the cytoplasm, whereas RFP-X_{CT} predominantly localized to the nucleus (Fig. 4d). These data indicate that the N-interacting X_{CT} domain is sufficient for symptom induction and virus accumulation.

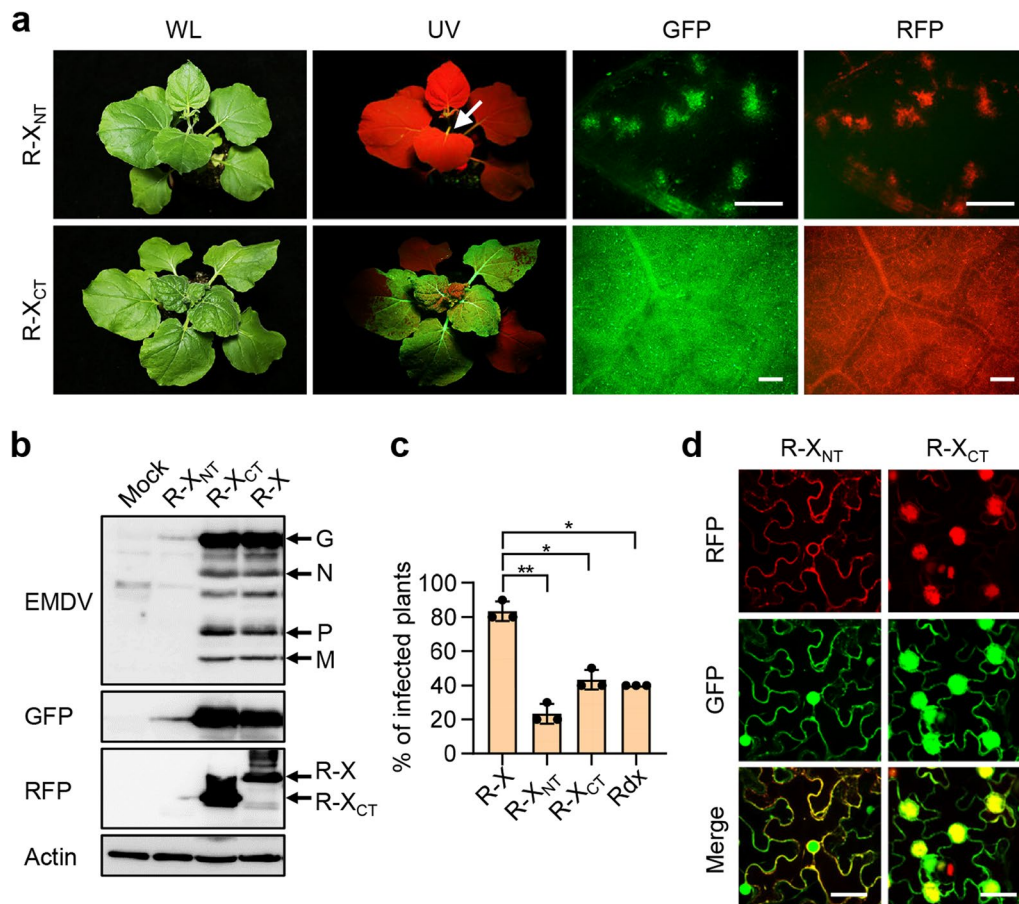


Fig. 4 Effects of X protein truncation on recombinant EMDV infections. **a** Symptoms and fluorescence in systematically infected *N. benthamiana* plants agroinfiltrated with EMDV constructs with the indicated X truncation. Infected plants and fluorescence patterns in leaf tissues were photographed at 30 dpi. Arrow indicates an infected young leaf petiole with faint GFP fluorescence. Scale bars: 500 μ m. **b** Accumulation of EMDV structural protein and fluorescent reporter proteins in infected leaf tissues detected by immunoblotting. The actin blot serves as a protein loading control. **c** Percentages of systemically infected *N. benthamiana* plants at 30 dpi. Data are shown as individual data points and mean \pm SD for 3 independent experiments ($n = 10$). Statistical P values were calculated using the two-tailed Student's t -test (**, $P < 0.01$; *, $P < 0.05$). **d** Confocal micrographs showing the localization patterns of RFP-X_{NT} and RFP-X_{CT} during EMDV R-X_{NT} or EMDV R-X_{CT} infections. Scale bars: 20 μ m

However, the full infectivity of EMDV also requires the X_{NT} domain.

Identification of the key amino acids of X protein involved in interaction with N and virus infection

To delineate the key region of X participating in interaction with N, we constructed a series of X mutants with stepwise C-terminal truncations (Fig. 5a) and

transiently co-expressed each mutant protein with CFP-N in *N. benthamiana* leaves. Through confocal microscopy analysis, we found that the X deletion mutant lacking the amino acids (aa) 71–83 region failed to be targeted to the nuclei by the co-expressed N protein (Fig. 5b). Co-IP and GST pull-down assays confirmed that deletion of this region abolished the interaction of X with N (Fig. 5c, d).

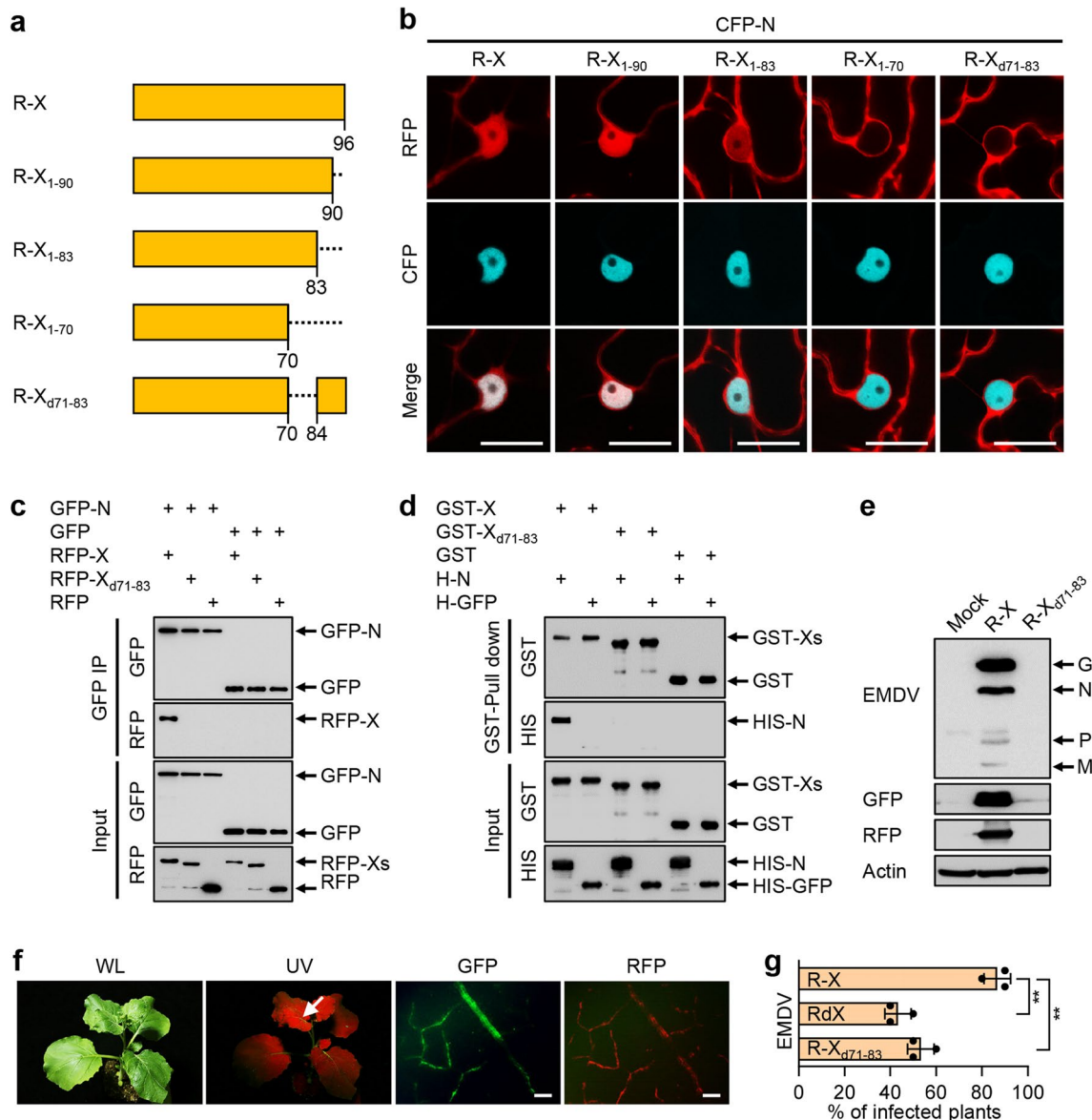


Fig. 5 Requirement of the N-X interaction for EMDV pathogenesis. **a** Illustration of the X protein deletion mutants fused with RFP. Dash lines denote the deleted region. **b** Confocal micrographs showing the subcellular localization of RFP-X derivatives co-expressed with CFP-N at 48 hpi. Scale bars: 20 μ m. **c, d** Co-IP and GST-Pull down assays for analyzing the interactions between X_{d71-83} and N. **e** Immunoblotting analysis of the accumulation of viral structural proteins and fluorescent proteins. **f** Symptom and fluorescence in *N. benthamiana* plants agroinfiltrated with EMDV R-X clone carrying the No. 71–88 aa truncation. Arrow indicates an upper leaf vein showing faint green fluorescence. Scale bars: 500 μ m. **g** Percentages of systemically infected *N. benthamiana* plants agroinoculated with the indicated EMDV derivative at 25 dpi

Next, we introduced this short deletion into the EMDV R-X clone, generating EMDV R-X_{d71-83}. Upon agroinoculation of *N. benthamiana* plants, EMDV R-X_{d71-83} exhibited infection characteristics reminiscent of EMDV RdX, including low levels of viral protein accumulation, asymptomatic infection, restricted vascular tissue distribution, and low infectivity (Fig. 5e–g). Taken together, these results indicate that X interaction with N through its aa 71–83 region is crucial for efficient EMDV infection and symptom induction in plants.

Heterologous X proteins can partially complement the functions of the EMDV X

Among the alphanucleorhabdoviruses-encoded X proteins, EMDV X was most closely related to PhCMoV X (63.5% aa identity), followed by CYDV X (44.8% identity) and PYDV X (34.3% identity). Alignment of the aa sequences of these X proteins identified a conserved region approximately 30 aa in length located in the C-termini of X, encompassing the aa 71–83 of EMDV X required for N interaction. Within this region, a consecutive stretch of seven aa (DNDSDIY) is identical among the four X proteins (Fig. 6a), suggesting that these heterologous X proteins might also interact with the EMDV N protein. To test this hypothesis, we co-expressed Y^N-fused EMDV N (Y^N-N) with Y^C-fused PhCMoV X (Y^C-PhX), CYDV X (Y^C-CYX), or PYDV X (Y^C-PYX) in the leaves of RFP-H2B *N. benthamiana* plants. Indeed, the BiFC results demonstrated that these heterologous X proteins interacted with the EMDV N protein, producing YFP fluorescence patterns similar to those observed with the EMDV X protein (Fig. 6b). These interactions were further confirmed by Co-IP assays (Fig. 6c). In both assays, CYDV X exhibited relatively weaker interactions with EMDV N than the other two X proteins, as indicated by the intensities of the YFP fluorescence (Fig. 6b) and the co-precipitated X protein products (Fig. 6c).

Next, we generated three chimeric EMDV constructs by replacing the X gene in EMDV R-X with each heterologous X genes. The chimeric clones were analyzed for their infection properties through agroinoculation of *N. benthamiana* plants. All three chimeric viruses induced symptoms indistinguishable from that of EMDV R-X (Fig. 6d) and produced abundant EMDV structural proteins (Fig. 6f). However, the CYDV X-containing EMDV produced reduced fluorescence in infected plant tissues (Fig. 6d, middle panels), consistent with its weak interactions with EMDV N (Fig. 6b, c). Additionally, although the closely related PhCMoV X fully complemented EMDV X in systemic infection, the distantly related PYDV and CYDV X provided only moderate levels of systemic infectivity (Fig. 6e).

Upon transient expression, the RFP-PhCMoV X fusion was exclusively targeted to the cytoplasm, similar to EMDV X. In contrast, RFP fusions of PYDV and CYDV X displayed both cytoplasmic and nuclear localization (Additional file 1: Figure S3a), as previously described (Bandyopadhyay et al. 2010; Jang et al. 2017). In the context of recombinant virus infections, all three X proteins were predominantly localized to the nucleus (Additional file 1: Figure S3b). Collectively, these data demonstrate that X proteins from related alphanucleorhabdoviruses can complement in varying degrees the functions of EMDV X.

Discussion

Some alphanucleorhabdoviruses encode a small X protein between the N/P gene junction, a position rarely contains accessory ORFs among plant- or animal-infecting rhabdoviruses (Walker et al. 2011, 2015; Beijerman et al. 2023). The lack of X positional analogs and sequence homologs has precluded the assignment of putative functions to these accessory proteins. In this study, we employed the recently established EMDV reverse genetics system (Wang et al. 2024) to investigate the role of the X proteins in virus infection. Our data show that EMDV X plays important roles in virus accumulation, symptom induction, and systemic infection. This study aligns with previous research demonstrating the significance of accessory proteins in the rhabdovirus life cycle. Examples include the C and C' proteins in vesiculoviruses and the distantly related paramyxoviruses (Peluso et al. 1996; Siering et al. 2022), the $\alpha 1$ proteins in ephemeroviruses (Joubert et al. 2014), the NV proteins in novirhabdoviruses (Purcell et al. 2012; He et al. 2021), and the P6/P9 proteins in cytorhabdoviruses (Gao et al. 2024).

We began the investigation first by analyzing the subcellular localization of EMDV X. The exclusive cytoplasmic localization of the ectopically expressed X protein was unexpected given its small size (~10 kDa), which should allow for free diffusion through the nuclear pore complexes. This cytoplasmic localization might be attributed to its association with the ER membrane or the presence of a putative nuclear export signal, which warrants further investigation. Nevertheless, in the context of EMDV infections, a significant fraction of the X protein was found to be translocated into the nucleus through specific interactions with the N protein. Additionally, X domain truncation and deletion analyses demonstrated that the localization of the X protein to the nucleus correlates with its pathogenic roles in EMDV infection. Nucleorhabdoviruses replicate and undergo virion morphogenesis within the infected nuclei, and the N protein is essential for encapsidating genomic RNAs to form nucleocapsids, for virus replication and mRNA

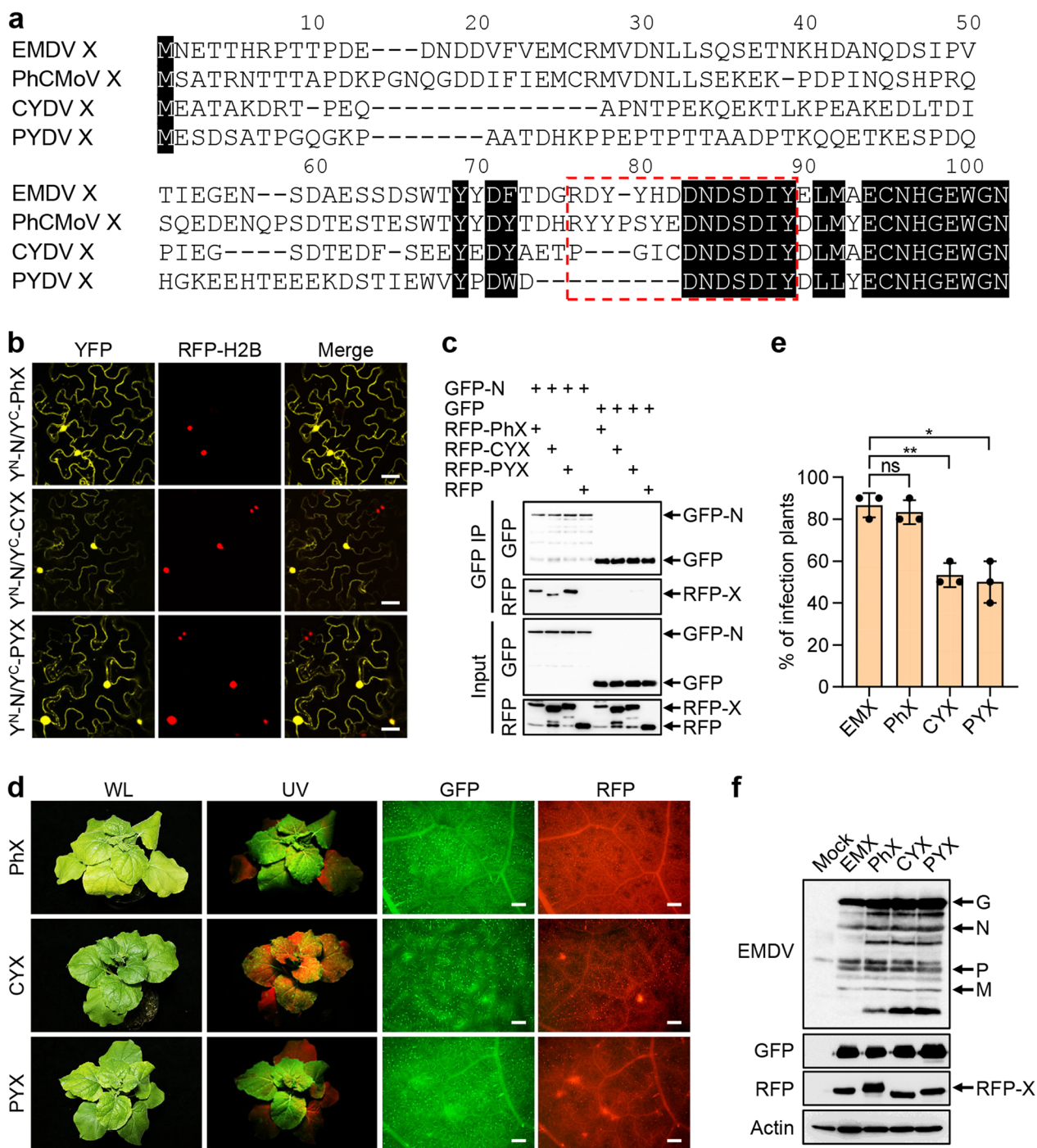


Fig. 6 Complementation of EMDV X by heterologous *Alphanucleorhabdovirus* X proteins. **a** Multiple sequence alignment of the X proteins. Red dashed box denotes the N-interacting region in EMDV X (No. 71 – 83 aa). **b, c** BiFC and Co-IP assays showing the interactions of EMDV N and the heterologous X proteins. Scale bars: 20 μ m. **d** Symptoms and fluorescence in *N. benthamiana* plants agroinoculated with the indicated chimeric EMDV, in which the native X gene was replaced by the RFP-tagged heterogonous X gene. Plants were photographed at 30 dpi. Scale bars: 500 μ m **e** Percentages of systemically infected plants at 30 dpi. **f** Western blot analysis of viral proteins and fluorescent proteins in upper leaf tissues of plants systemically infected with an EMDV derivative. The actin blot serves as a protein loading control

transcription, and it constitutes a major structural component of viroplasm and virus particles (Jackson et al. 2005). The specific N-X interaction suggests that X may facilitate EMDV infection by modulating virus replication and transcription. This hypothesis is supported by the greatly reduced levels of viral protein accumulation during infections of the X deletion mutant virus. Similar roles have been documented for the C and V accessory proteins encoded by some rhabdoviruses and paramyxoviruses, which associate with viral nucleocapsids and control polymerase processivity and orderly replication (Peluso et al. 1996; Grogan and Moyer 2001; Sweetman et al. 2001; Witko et al. 2006; Siering et al. 2022; Zhou et al. 2024). Recent work with several plant rhabdoviruses showed that the viroplasms, which house active virus replication, are biomolecular condensates formed through a liquid-liquid phase separation (Fang et al. 2019, 2022; Liang et al. 2023). We found that co-expression of the EMDV N and P proteins formed nuclear inclusions resembling viroplasms, and that RFP-X or RFP-X_{CT} was also recruited into these punctate structures (Additional file 1: Figure S4). These observations suggest a potential role of X in regulating virus replication, which requires further exploration in future studies.

We found that EMDV mutants lacking the entire X (EMDV RdX) or the X_{CT} domain (EMDV R-X_{NT}) were largely restricted in the vascular tissues, exhibiting an infection phenotype reminiscent of the M or G deletion mutants of sonchus yellow net virus (Wang et al. 2015; Sun et al. 2018; Ma and Li 2020). The M and G proteins of plant rhabdoviruses are crucial for driving virus budding collaboratively, and mutants lacking these proteins are deficient in virion morphogenesis or envelopment (Wang et al. 2015; Sun et al. 2018; Ma and Li 2020; Li and Zhao 2021). However, EMDV RdX mutant still produced enveloped, bacilliform particles, albeit in obviously reduced amounts. Furthermore, X was not identified in the purified virion preparations, which argues against direct involvement of X in virion budding. These data suggest that while X is not essential for virus particle assembly, it plays a significant role in facilitating the systemic spread of the virus within the host plant.

Deletion analyses showed that while EMDV R-X_{CT} behaved similarly to the wild-type virus in terms of symptom induction and virus protein accumulation, it displayed reduced infectivity compared with EMDV RdX. These findings suggest that the N-terminal domain of X plays additional roles in promoting systemic virus infection, likely mediated by its cytoplasmic localization signal. In supporting this, the EMDV X functions were fully complemented by PhCMoV X, which showed a similar cytoplasmic localization pattern (when expressed ectopically). By contrast, the CYDV and PYDV X proteins,

having a divergent C terminus sequence and lacking the nucleus-excluding localization, could only provide EMDV RdX with the roles in symptom induction and virus accumulation but not in systemic infection.

Accessory proteins of animal-infecting rhabdoviruses and paramyxoviruses often influence various biological processes of the host cells, particularly antiviral pathways. For example, the NV proteins of novirhabdoviruses facilitate viral pathogenesis through suppressing apoptosis (Ammayappan et al. 2011; Ammayappan and Vakharia 2011), blocking NF- κ B activation (Kim and Kim 2013), or antagonizing RIG-I-mediated interferon induction (Biacchesi et al. 2017). The C and V proteins of paramyxoviruses impair the innate immune responses by interfering with cellular transcription factors (Siering et al. 2022) or inactivating cytosolic pathogen recognition receptors (Ramachandran and Horvath 2010; Sánchez-Aparicio et al. 2018; Wagner et al. 2022). It remains to be determined whether the X proteins could interact with host antiviral pathways to promote viral pathogenesis.

Conclusions

Through reverse genetics, protein localization and interaction analyses, we showed that during EMDV infection, via interaction with the N protein, the X protein is transported into the nucleus where virus replication occurs. EMDV X protein is essential for viral pathogenesis, and the function is likely conserved between related alpha-nucleorhabdoviruses-encoded X proteins. Our data shed light on the roles of the poorly characterized accessory proteins of plant rhabdoviruses.

Methods

Plant material and plasmid construction

Nicotiana benthamiana wild type, 16c (Ruiz et al. 1998), and RFP-H2B (Martin et al. 2009) lines were grown at 25°C with 60% relative humidity under a 16-h light/8-h dark photoperiod. The plasmids used for the recovery of recombinant EMDV were described previously (Wang et al. 2024).

To generate RFP tagged derivatives, we amplified the full-length coding regions of DsRed, EMDV X, PhCMoV X, CYDV X, and PYDV X using gene-specific primers, and the truncated X_{NT}, X_{CT}, X₁₋₉₀, X₁₋₈₃, and X₁₋₇₀ sequences with the primer pairs EM X/BamH I/F and EM X_{NT}/Sal I/R, EM X_{CT}/BamH I/F and EM X/Sal I/R, EM X/BamH I/F and EM X₁₋₉₀/Sal I/R, EM X/BamH I/F and EM X₁₋₈₃/Sal I/R, EM X/BamH I/F and EM X₁₋₇₀/Sal I/R, respectively (Additional file 2: Table S1). Amplified fragments were then digested with *Bam*H I and *Sal* I and inserted between the pGD *Bam*H I and *Sal* I sites via T4 ligation (ThermoFisher Scientific, USA). Next, the DsRed fragments were amplified using the primer pairs

n-DsRed/15nt/F with n-DsRed/EM X/EM X_{CT}/Ph X/CY X/PY X/15nt/R and separately inserted into the *Bam*H I-digested pGD EM X, pGD EM X_{NT}, pGD EM X₁₋₉₀, pGD EM X₁₋₈₃, pGD EM X₁₋₇₀, pGD EM X_{CT}, pGD Ph X, pGD CY X, and pGD PY X plasmids by In-Fusion cloning (Vazyme, China) to obtain desired RFP tagged transient expression vectors. pGD RFP-X_{d71-83} was constructed through assembling two overlapping fragments amplified using pGD RFP-EM X as a template into *Bam*H I and *Sca*I linearized pGD EV via In-Fusion cloning.

To generate GFP- or CFP-tagged derivatives, the full-length coding sequences of GFP, EMDV Y, and EMDV M were each amplified using a specific forward primer containing the *Bam*H I restriction site and a reverse primer containing the *Sal*I site (Additional file 2: Table S1), followed by *Bam*H I and *Sal*I digestion and ligation into the pGD vector. Next, n-GFP fragments were amplified using the n-GFP/15nt/F and n-GFP/N/X/15nt/R primer pairs and separately inserted into the *Bam*H I-digested pGD EM-N and pGD EM-X plasmids by In-Fusion cloning to obtain pGD GFP-N and pGD GFP-X, respectively. For generation of CFP-tagged vectors, n-CFP fragments were amplified using the primer pairs n-GFP/15nt/F and n-GFP/N/P/Y/M/15nt/R and separately inserted into the *Bam*H I-linearized pGD EM-N, pGD EM-P, pGD EM-Y, and pGD EM-M plasmids, respectively, via In-Fusion cloning.

Constructs for BiFC assay were assembled by Gateway cloning. Full-length of coding sequences were amplified using specific primers with appended 5' Gateway attB sequence (Additional file 2: Table S1) and cloned into the entry vector pDONRTM221 (ThermoFisher Scientific) via BP recombination reactions. ORFs were then mobilized into the desired pSITE destination vectors (Martin et al. 2009) via LR cloning, as described previously (Liang et al. 2023).

Plasmids pET-32a EM-N and pET-32a GFP were obtained through inserting the N or GFP ORFs into the *Bam*H I and *Sac*I digested pET-32a plasmid via T4 ligation. pGEX-4T-3 EM-X and pGEX-4T-3 EM-X_{d71-83} were generated by inserting the X or X_{d71-83} ORFs into the *Bam*H I and *Sal*I linearized pGEX-4T-3 plasmid through T4 ligation.

To generate the pEMDV GFP X derivatives, an intermediate vector was generated with a modified 3.9 kb *Bst*B I-*Avr* II fragment from pEMDV GFP in which X ORF was replaced with two *Aar*I sites for subcloning of various X derivatives. Briefly, the primer pairs *Bst*B I/F with *Aar*I/18nt/R and *Aar*I/18nt/F with *Avr* II/R were used to amplify *Bst*B I-*Aar*I and *Aar*I-*Avr* II fragments, and these two overlapping fragments were assembled into pGD EV plasmid digested with *Bam*H I and *Sal*I via In-Fusion cloning to obtain the intermediate vector pGD

*Bst*B I-*Avr* II *Aar*I. The coding sequences of RFP, RFP-X, RFP-X_{NT}, RFP-X₁₋₉₀, RFP-X₁₋₈₃, RFP-X₁₋₇₀, RFP-X_{d71-83}, RFP-X_{CT}, RFP-Ph X, RFP-CY X, and RFP-PY X were amplified and inserted into the pGD *Bst*B I-*Avr* II *Aar*I plasmid through *Aar*I digestion. At last, *Bst*B I-*Avr* II fragments containing various X derivatives were inserted between pEMDV GFP *Bst*B I and *Avr* II sites via T4 ligation to generate the final pEMDV GFP X clones.

Agroinoculation of virus and agroinfiltration

The recovery of recombinant EMDV derivatives through agroinfiltration was performed as previously described (Wang et al. 2024).

For transient expression, plasmids were introduced into *A. tumefaciens* strain EHA105 by electroporation, followed by agroinfiltration of wild-type, 16c, or RFP-H2B *N. benthamiana* leaves at a final (OD)_{A600} of 0.2~0.3.

Fluorescence microscopy, confocal microscopy, and electron microscopy

GFP and RFP fluorescence in systematically infected *N. benthamiana* leaves were detected with a SteREO lumiar V12 epifluorescence microscope (Zeiss, Germany) with filter sets Lumiar 38 (470/40 nm excitation, 525/50 nm emission) and Lumiar 31 (565/30 nm excitation, 620/60 nm emission), respectively. Images were processed with ZEN 2.3 (Zeiss, Germany).

Subcellular localization and BiFC assays were performed with an FV3000 confocal laser scanning microscope (Olympus, Japan). CFP, GFP, YFP, and RFP fluorescence was separately excited at 405, 488, 514, and 561 nm. Images were processed with FV31S-SW (Olympus, Japan).

Sections of upper systemic leaf veins infected with EMDV viruses were observed under a transmission electron microscope (H-7650, Hitachi, Japan), as described previously (Wang et al. 2024).

Immunoblotting, co-immunoprecipitation (Co-IP), and GST pull-down

Total proteins were extracted and separated by 12.5% SDS-PAGE, and transferred to nitrocellulose membranes. Viral proteins on the blots were detected with a polyclonal antiserum raised against EMDV virions (1:5000; DSMZ, Germany) or monoclonal antibodies against GFP (1:8000; Abcam, UK), RFP (1:8000; MBL, China), or actin (1:5000; Sangon Biotech, China). Goat anti-mouse or anti-rabbit secondary antibodies (1:10,000; HuaAn, China) were used for detection of blots via digital imaging.

Co-IP assay was performed as described previously (Liang et al. 2023) with minor modifications. In brief, 0.5 g of *N. benthamiana* plant leaves were ground with

liquid nitrogen and extracted with 1 mL of Co-IP buffer (40 mM Tris-HCl [pH 7.5], 150 mM NaCl, 50 mM MgCl₂, 2% glycerol, 2 mM EDTA [pH 8.0], 5 mM dithiothreitol [DTT], 0.1% Triton X-100, and a protease inhibitor cocktail tablet [Roche]). Protein extracts were centrifuged for 15 min at 16,000×g. Supernatants were immunoprecipitated with 25 μL of anti-GFP magnetic beads (MBL, China) at 4°C for 3 h. Beads were then washed with Co-IP buffer for 5 times, and proteins attached to the beads were analyzed by immunoblotting.

GST Pull-down assay was conducted according to the protocol outlined by Kim and Hakoshima (Kim and Hakoshima 2019). 100 μL of glutathione resin (GenScript, China) was washed three times with Pull-down buffer (25 mM Tris-HCl [pH 7.4], 137 mM NaCl, 3 mM KCl, and protease inhibitor) via centrifugation at 500×g. Bait protein with a GST tag (2.5 μg) and prey protein (2.5 μg) were added to 50 μL of the washed resin. The total reaction volume was adjusted to 100 μL and incubated at 4°C for 15 min. A mixture of GST and prey protein was also incubated as a negative control. An aliquot (10 μL) of each mixture was extracted as the input component, while the remaining mixtures were washed with 5 bed volumes of assay buffer for 5 times through 500×g centrifugation. The resulting pellet was responded with 100 μL of assay buffer and served as the Pull-down component.

Membrane association assay

Subcellular extraction was performed as described previously (Zhou et al. 2019). Briefly, 0.5 g of leaves transiently expressing X derivatives were ground in 1 mL of lysis buffer (20 mM HEPES [pH 6.8], 150 mM potassium acetate, 250 mM mannitol, 1 mM MgCl₂, 1 mM DTT, and protease inhibitor) on ice, after which the protein extracts were centrifuged at 3000×g for 10 min at 4°C. The soluble and pellet fractions were marked as S3 and P3, respectively. The S3 fraction was further centrifuged at 30,000×g for 1 h at 4°C to separate the soluble (S30) and pellet (P30) fractions. For chemical treatments, the P30 fractions were divided into 5 aliquots, and 10 volumes of lysis buffer containing either 0.1 M Na₂CO₃ (pH 11.0), 1 M KCl, 4 M urea or 1% Triton X-100 were added to each aliquot of the P30 fraction and incubated for 30 min at 4°C. The samples were then centrifuged at 30,000×g for 1 h at 4°C again to obtain the soluble (S) and pellet (P) fractions. Immunoblotting was performed for analysis of the membrane association types.

Nuclear-cytoplasmic fraction assay

Nuclear-cytoplasmic fractionation was conducted as described previously (Mei et al. 2018). *N. benthamiana*

leaves (0.5 g) were gently ground with 500 μL of lysis buffer (20 mM Tris-HCl [pH 7.5], 20 mM KCl, 2 mM MgCl₂, 25% glycol [v/v], 250 mM sucrose, and 5 mM DTT) and centrifuged at 1500×g for 10 min at 4°C. The resulting supernatant was further centrifuged at 10,000×g for 10 min at 4°C to generate the cytoplasmic fraction. The pellet was washed for 6 times with NRBT buffer (20 mM Tris-HCl [pH 7.4], 2.5 mM MgCl₂, 25% glycol, 0.2% Triton X-100), resuspended in 500 μL of NRB2 buffer (20 mM Tris-HCl [pH 7.5], 10 mM MgCl₂, 250 mM sucrose, 0.5% Triton X-100, 5 mM β-mercaptoethanol [β-ME]), and then carefully mixed with 500 μL of NRB3 buffer (20 mM Tris-HCl [pH 7.5], 10 mM MgCl₂, 1.7 M sucrose, 0.5% Triton X-100, 5 mM β-ME). The mixture was centrifuged at 16,000×g for 45 min at 4°C, and the nuclear fraction is recovered by resuspending the resulting pellet in 400 μL of lysis buffer. All buffers used in the nuclear-cytoplasmic fraction assay contained protease inhibitor.

Abbreviations

| | |
|--------|------------------------------------|
| aa | Amino acid(s) |
| BYSMV | Barley yellow striate mosaic virus |
| CFP | Cyan fluorescent protein |
| CYDV | Constricta yellow dwarf virus |
| dpi | Days post inoculation |
| EMDV | Eggplant mottled dwarf virus |
| GFP | Green fluorescent protein |
| hpi | Hours post infiltration |
| ORF | Open reading frame |
| PhCMoV | Physostegia chlorotic mottle virus |
| PYDV | Potato yellow dwarf virus |
| RFP | Red fluorescent protein |
| YFP | Yellow fluorescent protein |

Supplementary Information

The online version contains supplementary material available at <https://doi.org/10.1186/s42483-024-00280-7>.

Additional file 1: Figure S1. Microsomal association analysis of the EMDV X protein. **Figure S2.** Confocal micrographs showing the localization of the RFP tagged X_{NT} and X_{CT}. **Figure S3.** Subcellular localization of X proteins encoded by additional alphanucleorhabdoviruses. **Figure S4.** Recruitment of EMDV X and X_{CT} into the nuclear N-P inclusion bodies.

Additional file 2: Table S1. Primers used in this study.

Acknowledgements

We thank Dr. Yaqin Wang and Dr. Li Xie, and Ms. Yunqin Li (Zhejiang University) for assistance in confocal microscopy and transmission electron microscopy.

Author contributions

ZL and SW designed the research; SW, HL, and SN performed the experiments; SW, HL, and YL analyzed the data; ZL and SW wrote the paper. All authors read and approved the final manuscript.

Funding

This work was supported by grant from the National Key R&D Program of China (2023YFD1400300) and the Natural Science Foundation of Zhejiang Province, China (LZ20C140004) to ZL.

Availability of data and materials

The data and materials that support the findings of this study are available from the corresponding author upon request.

Declarations**Ethics approval and consent to participate**

Not applicable.

Consent for publication

Not applicable.

Competing interests

The authors declare that they have no competing interests.

Received: 17 June 2024 Accepted: 22 August 2024

Published online: 19 November 2024

References

- Alfaro-Fernández A, Córdoba-Sellés C, Tornos T, Cebrián MC, Font MI. First report of eggplant mottled dwarf virus in *Pittosporum tobira* in Spain. *Plant Dis.* 2011;95:75–75. <https://doi.org/10.1094/PDIS-07-10-0491>.
- Ammayappan A, Vakharia VN. Nonvirion protein of novirhabdovirus suppresses apoptosis at the early stage of virus infection. *J Virol.* 2011;85:8393–402. <https://doi.org/10.1128/jvi.00597-11>.
- Ammayappan A, Kurath G, Thompson TM, Vakharia VN. A reverse genetics system for the Great Lakes strain of viral hemorrhagic septicemia virus: the NV gene is required for pathogenicity. *Mar Biotechnol.* 2011;13:672–83. <https://doi.org/10.1007/s10126-010-9329-4>.
- Babaie G, Kouhi HM, Massah A, Dizadji A, Izadinejad L, Simon A. Complete genome sequence and genome analysis of eggplant mottled dwarf virus-Iranian isolate. *J Phytopathol.* 2014;63:331–41. <https://doi.org/10.1111/jph.12256>.
- Bandyopadhyay A, Kopperud K, Anderson G, Martin K, Goodin M. An integrated protein localization and interaction map for potato yellow dwarf virus, type species of the genus *Nucleorhabdovirus*. *Virology.* 2010;402:61–71. <https://doi.org/10.1016/j.virol.2010.03.013>.
- Bejerman NE, Dietzgen RG, Debat H. Illuminating the plant rhabdovirus landscape through metatranscriptomics data. *Viruses.* 2021;13(7):1304. <https://doi.org/10.3390/v13071304>.
- Bejerman NE, Dietzgen RG, Debat H. Novel tri-segmented rhabdoviruses: a data mining expedition unveils the cryptic diversity of cytorhabdoviruses. *Viruses.* 2023;15(12):2402. <https://doi.org/10.3390/v15122402>.
- Biacchesi S, Méroux E, Chevret D, Lamoureux A, Bernard J, Brémont M. NV proteins of fish novirhabdovirus recruit cellular PPM1B protein phosphatase and antagonize RIG-I-mediated IFN induction. *Sci Rep.* 2017;7:44025. <https://doi.org/10.1038/srep44025>.
- Dietzgen RG, Bejerman NE, Goodin MM, Higgins CM, Huot OB, Kondo H, et al. Diversity and epidemiology of plant rhabdoviruses. *Virus Res.* 2020;281:197942. <https://doi.org/10.1016/j.virusres.2020.197942>.
- Dietzgen RG, Bejerman NE, Mei Y, Jee CLJ, Chabi-Jesus C, Freitas-Astúa J, et al. Joá yellow blotch-associated virus, a new *Alphanucleorhabdovirus* from a wild solanaceous plant in Brazil. *Arch Virol.* 2021a;166:1615–22. <https://doi.org/10.1007/s00705-021-05040-y>.
- Dietzgen RG, Goodin MM, Li ZH. Plant Rhabdoviruses (*Rhabdoviridae*). In: *Encyclopedia of virology* (Fourth Edition). Oxford: Academic Press, Elsevier; 2021. <https://doi.org/10.1016/B978-012374410-4.00492-1>.
- Fang XD, Yan T, Gao Q, Cao Q, Gao DM, Xu WY, et al. A cytorhabdovirus phosphoprotein forms mobile inclusions trafficked on the actin/ER network for viral RNA synthesis. *J Exp Bot.* 2019;70:4049–62. <https://doi.org/10.1093/jxb/erz195>.
- Fang XD, Gao Q, Zang Y, Qiao JH, Gao DM, Xu WY, et al. Host casein kinase 1-mediated phosphorylation modulates phase separation of a rhabdovirus phosphoprotein and virus infection. *Elife.* 2022;11:e74884. <https://doi.org/10.7554/eLife.74884>.
- Gao DM, Zhang ZJ, Qiao JH, Gao Q, Zang Y, Xu WY, et al. A rhabdovirus accessory protein inhibits jasmonic acid signaling in plants to attract insect vectors. *Plant Physiol.* 2022;190:1349–64. <https://doi.org/10.1093/plphys/kiac319>.
- Gao DM, Qiao JH, Gao Q, Zhang J, Zang Y, Xie L, et al. A plant cytorhabdovirus modulates locomotor activity of insect vectors to enhance virus transmission. *Nat Commun.* 2023;14:5754. <https://doi.org/10.1038/s41467-023-41503-3>.
- Gao Q, Zang Y, Qiao JH, Zhang ZY, Wang Y, Han CG, et al. The plant rhabdovirus viroporin P9 facilitates insect-mediated virus transmission in barley. *Plant Cell.* 2024. <https://doi.org/10.1093/plcell/koae162>.
- Grogan CC, Moyer SA. Sendai virus wild-type and mutant C proteins show a direct correlation between L polymerase binding and inhibition of viral RNA synthesis. *Virology.* 2001;288:96–108. <https://doi.org/10.1006/viro.2001.1068>.
- Haseloff J, Siemering KR. The uses of green fluorescent protein in plants. *Methods Biochem Anal.* 2006;47:259–84. <https://doi.org/10.1002/047139499.ch12>.
- He M, Ding NZ, He CQ. Novirhabdoviruses versus fish innate immunity: a review. *Virus Res.* 2021;304:198525. <https://doi.org/10.1016/j.virusres.2021.198525>.
- Huang YW, Geng YF, Ying XB, Chen XY, Fang RX. Identification of a movement protein of rice yellow stunt rhabdovirus. *J Virol.* 2005;79:2108–14. <https://doi.org/10.1128/JVI.79.4.2108-2114.2005>.
- Jackson AO, Dietzgen RG, Goodin MM, Bragg JN, Deng M. Biology of plant rhabdoviruses. *Annu Rev Phytopathol.* 2005;43:623–60. <https://doi.org/10.1146/annurev.phyto.43.011205.141136>.
- Jang C, Wang R, Wells J, Leon F, Farman M, Hammond J, Goodin MM. Genome sequence variation in the constricta strain dramatically alters the protein interaction and localization map of potato yellow dwarf virus. *J Gen Virol.* 2017;98:1526–36. <https://doi.org/10.1099/jgv.0.000771>.
- Joubert DA, Blasdel KR, Audsley MD, Trinidad L, Monaghan P, Dave KA, et al. Bovine ephemeral fever rhabdovirus a1 protein has viroporin-like properties and binds Importin β 1 and Importin 7. *J Virol.* 2014;88:1591–603. <https://doi.org/10.1128/JVI.01812-13>.
- Kim SY, Hakoshima T. GST Pull-Down assay to measure complex formations. *Methods Mol Biol.* 2019;1893:273–80. https://doi.org/10.1007/978-1-4939-8910-2_20.
- Kim MS, Kim KH. The role of viral hemorrhagic septicemia virus (VHSV) NV gene in TNF- α and VHSV infection-mediated NF- κ B activation. *Fish Shellfish Immunol.* 2013;34:1315–9. <https://doi.org/10.1016/j.fsi.2013.02.026>.
- Kuzmin IV, Novella IS, Dietzgen RG, Padhi A, Rupprecht CE. The rhabdoviruses: biodiversity, phylogenetics, and evolution. *Infect Genet Evol.* 2009;9(4):541–53. <https://doi.org/10.1016/j.meegid.2009.02.005>.
- Li Z, Zhao C. Plant negative-stranded RNA virus biology and host interactions revitalized by reverse genetics. *Curr Opin Virol.* 2021;48:1–9. <https://doi.org/10.1016/j.coviro.2021.03.003>.
- Liang Y, Zhang X, Wu B, Wang S, Kang L, Deng Y, et al. Actomyosin-driven motility and coalescence of phase-separated viral inclusion bodies are required for efficient replication of a plant rhabdovirus. *New Phytol.* 2023;240:1990–2006. <https://doi.org/10.1111/nph.19255>.
- Ma X, Li Z. Significantly improved recovery of recombinant sonchus yellow net rhabdovirus by expressing the negative-strand genomic RNA. *Viruses.* 2020;12(12):1459. <https://doi.org/10.3390/v12121459>.
- Mann KS, Bejerman N, Johnson KN, Dietzgen RG. Cytorhabdovirus P3 genes encode 30K-like cell-to-cell movement proteins. *Virology.* 2016;489:20–33. <https://doi.org/10.1016/j.virol.2015.11.028>.
- Martin K, Kopperud K, Chakrabarty R, Banerjee R, Brooks R, Goodin MM. Transient expression in *Nicotiana benthamiana* fluorescent marker lines provides enhanced definition of protein localization, movement and interactions in planta. *Plant J.* 2009;59:150–62. <https://doi.org/10.1111/j.1365-3113X.2009.03850.x>.
- Maurino F, Dumón AD, Llauger G, Alemandri V, de Haro LA, Mattio MF, et al. Complete genome sequence of maize yellow striate virus, a new cytorhabdovirus infecting maize and wheat crops in Argentina. *Arch Virol.* 2018;163(1):291–5. <https://doi.org/10.1007/s00705-017-3579-7>.
- Mavrič I, Žnidarič MT, Marn MV, Dolničar P, Mehle N, Lesemann DE, et al. First report of eggplant mottled dwarf virus in potato and tomato in Slovenia. *Plant Pathol.* 2006;55:566. <https://doi.org/10.1111/j.1365-3059.2006.01414.x>.
- McWilliam SM, Kongsuwan K, Cowley JA, Byrne KA, Walker PJ. Genome organization and transcription strategy in the complex GNS-L intergenic region

- of bovine ephemeral fever rhabdovirus. *J Gen Virol.* 1997;78:1309–17. <https://doi.org/10.1099/0022-1317-78-6-1309>.
- Mei Y, Wang Y, Hu T, Yang X, Lozano-Duran R, Sunter G, et al. Nucleocytoplasmic shuttling of geminivirus C4 protein mediated by phosphorylation and myristoylation is critical for viral pathogenicity. *Mol Plant.* 2018;11:1466–81. <https://doi.org/10.1016/j.molp.2018.10.004>.
- Menzel W, Richert-Pöggeler KR, Winter S, Knierim D. Characterization of a nucleorhabdovirus from *Physostegia*. *Acta Hort.* 2018;1193:29–38. <https://doi.org/10.17660/ActaHortic.2018.1193.5>.
- Peluso RW, Richardson JC, Talon J, Lock M. Identification of a set of proteins (C' and C) encoded by the bicistronic P gene of the Indiana serotype of vesicular stomatitis virus and analysis of their effect on transcription by the viral RNA polymerase. *Virology.* 1996;218:335–42. <https://doi.org/10.1006/viro.1996.0202>.
- Purcell MK, Laing KJ, Winton JR. Immunity to fish rhabdoviruses. *Viruses.* 2012;4:140–66. <https://doi.org/10.3390/v4010140>.
- Ramachandran A, Horvath CM. Dissociation of paramyxovirus interferon evasion activities: universal and virus-specific requirements for conserved V protein amino acids in MDA5 interference. *J Virol.* 2010;84(21):11152–63. <https://doi.org/10.1128/JVI.01375-10>.
- Ruiz MT, Voynet O, Baulcombe DC. Initiation and maintenance of virus-induced gene silencing. *Plant Cell.* 1998;10:937–46. <https://doi.org/10.1105/tpc.10.6.937>.
- Sánchez-Aparicio MT, Feinman LJ, García-Sastre A, Shaw ML. Paramyxovirus V proteins interact with the RIG-I/TRIM25 regulatory complex and inhibit RIG-I signaling. *J Virol.* 2018;92(6):e01960–e2017. <https://doi.org/10.1128/JVI.01960-17>.
- Siering O, Cattaneo R, Pfaller CK. C proteins: controllers of orderly paramyxovirus replication and of the innate immune response. *Viruses.* 2022;14(1):137. <https://doi.org/10.3390/v14010137>.
- Sun K, Zhou X, Lin W, Zhou X, Jackson AO, Li Z. Matrix-glycoprotein interactions required for budding of a plant nucleorhabdovirus and induction of inner nuclear membrane invagination. *Mol Plant Pathol.* 2018;19(10):2288–301. <https://doi.org/10.1111/mpp.12699>.
- Sweetman DA, Miskin J, Baron MD. Rinderpest virus C and V proteins interact with the major (L) component of the viral polymerase. *Virology.* 2001;281:193–204. <https://doi.org/10.1006/viro.2000.0805>.
- Wagner ND, Liu H, Rohrs HW, Amarasinghe GK, Gross ML, Leung DW. Nipah virus V protein binding alters MDA5 helicase folding dynamics. *ACS Infect Dis.* 2022;8(1):118–28. <https://doi.org/10.1021/acscinfecdis.1c00403>.
- Walker PJ, Dietzgen RG, Joubert DA, Blasdel KR. Rhabdovirus accessory genes. *Virus Res.* 2011;162:110–25. <https://doi.org/10.1016/j.virusres.2011.09.004>.
- Walker PJ, Firth C, Widen SG, Blasdel KR, Guzman H, Wood TG, et al. Evolution of genome size and complexity in the *Rhabdoviridae*. *PLoS Pathog.* 2015;11(2): e1004664. <https://doi.org/10.1371/journal.ppat.1004664>.
- Walker PJ, Freitas-Astúa J, Bejerman N, Blasdel KR, Breyta R, Dietzgen RG, et al. ICTV virus taxonomy profile: *Rhabdoviridae* 2022. *J Gen Virol.* 2022;103: 001689. <https://doi.org/10.1099/jgv.0.001689>.
- Wang Q, Ma X, Qian S, Zhou X, Sun K, Chen X, et al. Rescue of a plant negative-strand RNA virus from cloned cDNA: insights into enveloped plant virus movement and morphogenesis. *PLoS Pathog.* 2015;11(10):e1005223. <https://doi.org/10.1371/journal.ppat.1005223>.
- Wang S, Chen B, Ni S, Liang Y, Li Z. Efficient generation of recombinant eggplant mottled dwarf virus and expression of foreign proteins in solanaceous hosts. *Virology.* 2024;591: 109980. <https://doi.org/10.1016/j.viro.2024.109980>.
- Witko SE, Kotash C, Sidhu MS, Udem SA, Parks CL. Inhibition of measles virus minireplicon-encoded reporter gene expression by V protein. *Virology.* 2006;348:107–19. <https://doi.org/10.1016/j.viro.2005.12.019>.
- Yamada K, Fuji K, Shimada T, Nishimura M, Hara-Nishimura I. Endosomal proteases facilitate the fusion of endosomes with vacuoles at the final step of the endocytotic pathway. *Plant J.* 2005;41(6):888–98. <https://doi.org/10.1111/j.1365-313X.2005.02349.x>.
- Yan T, Zhu JR, Di D, Gao Q, Zhang Y, Zhang A, et al. Characterization of the complete genome of barley yellow striate mosaic virus reveals a nested gene encoding a small hydrophobic protein. *Virology.* 2015;478:112–22. <https://doi.org/10.1016/j.viro.2014.12.042>.
- Zhou X, Lin W, Sun K, Wang S, Zhou X, Jackson AO, et al. Specificity of plant rhabdovirus cell-to-cell movement. *J Virol.* 2019;93:e00296–e319. <https://doi.org/10.1128/JVI.00296-19>.
- Zhou L, Kang HX, Xu SY, Chen JB, Wang XY, Long HS, et al. Tailam paramyxovirus C protein inhibits viral replication. *J Virol.* 2024;98: e0165423. <https://doi.org/10.1128/jvi.01654-23>.